# DETERMINATION OF NEUTRON FLUX SPECTRUM BY THIN FOIL ACTIVATION

by

Glenn Earl Russcher

A Thesis Submitted to the
Graduate Faculty in Partial Fulfillment of
The Requirements for the Degree of
MASTER OF SCIENCE

Major Subject: Nuclear Engineering



Iowa State University
Of Science and Technology
Ames, Iowa

1962

# TABLE OF CONTENTS

# INTRODUCTION

Since nuclear reactors have been developed, concern has been expressed over the effects resulting from exposure to the neutron flux generated by them. The only means of standardizing the data collected from these early reactors and experiments was to perform the experiments in a thermal column or in some facility that provided a flux of essentially thermalized neutrons. These data collected by rather simple counting devices provided useful information in many fields such as the radiation effects of thermal neutrons, neutron activated reactions, and thermal cross section studies.

However, when an attempt was made to expand these methods to utilize the fast neutron flux present in the reactor core region, no convenient means of evaluating the neutron flux spectrum was available. As a result, a large quantity of data was collected, but many contradictory results were published. At best, results were correlated to integrated flux time, with no attempt made to estimate the flux spectrum.

# LITERATURE REVIEW

After it was discovered that neutrons are susceptable to Bragg reflection, suggesting the possibility of producing a monochromatic beam of neutrons by means of diffraction in a large single crystal, Zinn (1) developed a crystal monochromator at Argonne. This device could separate a small nearly monochromatic neutron beam from an external neutron flux spectrum. However, the major disadvantage of this device is its poor resolution at high energies. For that reason it is normally used for separating neutrons of energy less than 10 ev. Hence crystal monochromators are not well suited for reactor flux spectrum determination.

A second apparatus which also selects a particular energy segment from a neutron spectrum is a mechanical, velocity sensitive selector commonly known as a neutron chopper (2). However, unlike the crystal monochromator, neutron choppers are used well into the fast neutron range. Neutron choppers have the additional advantage of smaller size. In spite of this size advantage, the neutron chopper is not well suited to reactor measurements either, for many radiation cavities such as pneumatic tubes are inaccessible or simply too small for the chopper and its associated equipment. Another consideration, perhaps even more serious, is the distortion that such an apparatus would cause in the

surrounding neutron flux spectrum since the collimator and shutters of the neutron chopper must necessarily be neutron poisons.

Thus it is evident that the first two methods of neutron spectra measurement are useful only at reactor beam ports or at similar sources of an external neutron beam, hence they will not be discussed further.

Some measure of success has been shown, however, in the use of thin foils for determining the neutron flux spectrum in radiation cavities. Thin foils are small and durable enough to be introduced into the core region by means of a pneumatic tube, but may still be kept thin enough that the surrounding neutron flux is not disturbed. Since foil activation techniques seem to offer the most promise for neutron flux spectrum determination, several avenues of approach have been investigated.

The most prevalent approach utilizes a series of threshold reactions to obtain values of the neutron flux above the respective threshold energies. Representative investigations of this type have been published by Fischer (3) who used the fission threshold reactions of $U^{234}$, $U^{235}$, $U^{236}$, $U^{238}$ and by Grader (4) who used the fission threshold reactions of $Pu^{239}$ and $U^{238}$ as well as the threshold $S^{32}(n,p)\ P^{32}$ reaction. Grader measured the neutron flux spectrum of the LPTR and the KEWB-1 reactors with an estimated accuracy of

about 5 per cent, within the accuracy of the cross sections, and found a strong correlation with the fission spectrum.

The principal disadvantages of the threshold reaction approach lie in the many hazards associated with the use of fissionable isotopes of U and Pu. The use of non-fissionable threshold reactions would be much more convenient; however, the lack of information concerning threshold reactions below 1 Mev leaves only the anticipation of what might be done if such reactions are discovered. At present the well known non-fissionable threshold reactions almost all occur in the energy range from 1 to 10 Mev, hence are hardly adaptable to neutron flux spectrum measurements over the range from thermal energy to 10 Mev.

A second method of approach utilizing foil activation techniques is represented by the publication of Pai et al. (5). This method utilizes the assumption that for some materials such as In, which have large resonance cross section peaks, the total activation cross section may be approximated by the resonance peak cross section and the neutron flux at the energy of the resonance peak. The foil activation is measured and the resonance peak cross section is obtained from Hughes and Schwartz (6). Thus an approximation of the neutron flux at 1.45 ev is obtained. In a similar way the flux is found at the resonance peak energies of Ag 5.2 ev, Mn 340 ev, etc. A curve drawn through these points

is a representation of the neutron flux spectrum. This system has many advantages; however, its primary disadvantage lies in the basic assumption, "the total activation cross section may be approximated by the resonance peak cross section alone."

In the case of In, the area under the resonance peak on an energy versus cross section per unit energy curve is about 94 per cent of the area under the entire curve. However in the case of Mn, the area under the resonance peak is only 55 per cent of the area under the entire curve. This would tend to indicate the magnitude of the error involved in such an assumption.

# THEORY

Since it is desired to develop a method of determining the neutron flux spectrum at various positions within the reactor, assumptions usually associated with the continuous slowing-down model are no longer valid. For example, the pneumatic rabbit tube near the core cannot be considered an infinite, homogeneous, non-absorbing medium, therefore the usual procedure of considering only energies well below the source energy can not be used. The flux spectrum at the pneumatic rabbit tube will probably range from near the maximum fission energy to thermal.

An approximation to such a flux spectrum could be made by dividing the energy range into several segments, then measuring an average value of the flux in each segment. An experimental value of the thermal flux as found from bare and Cd covered Au activity, is used as an approximation of the flux below the cadmium cut-off. Similarly, an experimental value of the fast flux above 2.1 Mev is found from the activation of Al due to its threshold reaction (7). The flux in the remaining energy interval from 0.4 ev to 2.1 Mev is approximated by an average value in each of six energy segments. The first segment covers the range from 0.4 ev to 10 ev, the second from 10 ev to 100 ev etc. The third, fourth, and fifth segments are all energy decades, but the

sixth extends from 0.1 Mev to 2.1 Mev.

These six average values of the flux are derived from the simultaneous solution of the activation equation for six different materials. The total activation of a material is a summation of the activation caused by each energy interval of the flux.

$$A_T = A_{th} + \sum_{i=1}^{6} \bar{\phi}_i f_i ave(E, a, \Theta) + A_f$$

$f_i ave(E, a, \Theta)$ is defined as the activation function, and is dependent on the energy, the activation cross section and the incident angle of the neutron into the foil. Since the total activity $A_T$ may be found experimentally for each of the six materials, six equations will result which can be solved for the six values of $\bar{\phi}_i$, providing that values of $f_i ave$ can be evaluated for each material in each energy interval.

The following development of $f_i ave$ is based on the presentation by Hwang (8). One basic assumption is that all scattering processes are spherically symmetric in the center of mass system. This assumption is strictly valid for the energy range below 1 Mev (9).

A second more intuitive assumption is that the neutron flux at all energies is assumed to be uniformly distributed at the surface of the foil.

A final assumption which is necessary for the validity

of the experimental procedure is the assumption that the flux spectrum is percentage-wise independent of the power level of the reactor, within its normal operating range, i.e., it is assumed that the percentage of the neutron flux which falls within the energy range from, say, 1-10 ev will be the same whether the reactor is operating at 0.1 watt or 10,000 watts.

In the development of the activation function, consider first the probability of neutron scattering into the elemental area at a distance of r from the point of scatter. This area also corresponds to the element of solid angle subtended by the area at the point of scatter.

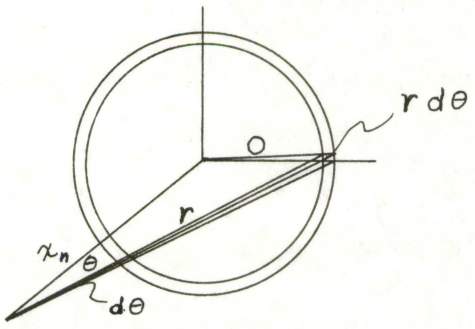


$$\sin\theta = \frac{O}{r} \therefore O = r\sin\theta$$

The probability of scattering within an angle $\theta$ is equal to

$$P_1 = \int_0^{\theta} \frac{(2\pi r\sin\theta)(r\,d\theta)}{4\pi r^2} = \int_0^{\theta} \frac{\sin\theta\,d\theta}{2} = -\int_1^{\mu} \frac{d\mu}{2}$$

since cos $\theta$ is commonly denoted by $\mu$. Also the probability that a neutron traveling the distance r will not be absorbed or scattered is

$$P_2 \times P_3 = \left(e^{-\Sigma_a r}\right)\left(e^{-\Sigma_a r}\right) = \left(e^{\frac{-\Sigma_a x_n}{\cos\theta}}\right)\left(e^{\frac{-\Sigma_s x_n}{\cos\theta}}\right)$$

The probability that the neutron will be absorbed but not scattered is

$$P_4 = \left(e^{\frac{-\Sigma_s x_n}{\cos\theta}}\right)\left(1 - e^{\frac{-\Sigma_a x_n}{\cos\theta}}\right)$$

Then the total probability of neutron absorption P per unit area of foil due to the neutron current is the rate of absorption R in the lethargy interval $u_2 - u_1$.

$$R = \int_{u_1}^{u_2} \int_{-1}^{1} \phi(u)\,\mu\left(1 - e^{\frac{-\Sigma_a x_n}{\cos\theta}}\right)\left(e^{\frac{-\Sigma_s x_n}{\cos\theta}}\right)\frac{d\mu}{2}\,du$$

$\bar{\phi}(\bar{\xi})$ is a mean value of $\phi(u)$ and may be considered a constant on the basis of the mean value theorem. Thus:

$$R = \bar{\phi}(\bar{\xi}) \int_{E_1}^{E_2} \int_{\epsilon}^{1} \left(1 - e^{\frac{-\Sigma_a x_n}{\mu}}\right)\left(e^{\frac{-\Sigma_s x_n}{\mu}}\right)\mu\,d\mu\,\frac{dE}{E} \qquad (\epsilon > 0)$$

Since the value of $\frac{\Sigma_s x_n}{\mu}$ is very small for the materials of interest, the probability $e^{\frac{-\Sigma_s x_n}{\mu}}$ may be assumed to be unity. Similarly $\frac{\Sigma_a x_n}{\mu}$ is also small, however it is still of significant size. Therefore since $\frac{\Sigma_a x_n}{\mu} \ll 1$ and $\mu > 0$ for all regions except the principal resonance regions, $\left(1 - e^{\frac{-\Sigma_a x_n}{\mu}}\right)$

may be expanded into a power series

$$\left(1 - e^{-\frac{\Sigma_a x_n}{\mu}}\right) = 1 - \left[1 - \frac{\Sigma_a x_n}{\mu} + \left(\frac{\Sigma_a x_n}{\mu}\right)^2 + \ldots\right]$$

If only the first two terms of this expansion are considered,

$$R = \frac{A}{a_n} = \bar{\Phi}(\bar{\xi}) \int_{\epsilon}^{1} \int_{E_1}^{E_2} \frac{\Sigma_a x_n}{\mu} \frac{dE}{E} \mu d\mu$$

$$= \bar{\Phi}(\bar{\xi})\, x_n \int_{E_1}^{E_2} \frac{\Sigma_a}{E} dE.$$

Since $x_n$ is the thickness of the foil and $a_n$ is the surface area of the foil, $x_n a_n = V_n$ the volume of the foil. A is activation.

$$\therefore A = \frac{V_n \rho N_o}{At} \bar{\Phi}(\bar{\xi}) \int_{E_1}^{E_2} \frac{\sigma_a}{E} dE = V_n N \bar{\Phi}(\bar{\xi}) \int_{E_1}^{E_2} \frac{\sigma_a}{E} dE$$

Where $N_o$ is Avogadro's number and N is the number of nuclei/$cm^3$, then for energy regions not containing the principal resonance, the activation function is

$$f_{1_1} = V_n N \int_{E_1}^{E_2} \frac{\sigma_a}{E} dE \qquad (1)$$

However for the energy region around the significant resonance peaks, the activation function is

$$f_{i_2} = a_n \int_{E_1}^{E_2} \int_{\epsilon}^{1} \left(1 - e^{\frac{-\Sigma_a x_n}{\mu}}\right) \mu \, d\mu \, \frac{dE}{E} \qquad (2)$$

Since this activation function must be considered wherever $\Sigma_a x_n \ll 1$ is not true, a demarkation value of 0.01 is chosen. Hence for each of the materials chosen, when the value of $\Sigma_a x$ exceeds 0.01, the relation 2 must be evaluated rather than relation 1. Then the average value of the activation function to be used in the energy interval as for example from 1-10 ev;

$$\bar{F}_i = f_{i_1}(1 - A) + f_{i_2}(A - B) + f_{i_1}(B - 10)$$

where $f_{i_1}(1 - A)$ and $f_{i_1}(B - 10)$ are found by use of relation 1 and $f_{i_2}(A - B)$ is found by means of relation 2.

In each of the activation functions to be evaluated, the $(n, \gamma)$ absorption cross section $\sigma_a$ must be determined as a function of energy. Total cross sections are published as a function of energy (6, 10). The total cross section is the summation of the $(n, \gamma)$ absorption cross section $\sigma_a$, the potential scattering cross section $\sigma_p$, the resonance scattering cross section $\sigma_{rs}$, the inelastic scattering cross section $\sigma_{ie}$ and many others. Those which are not significant at energies below 1 Mev will not be considered here, even though they are included in the total cross section.

The method of evaluating the absorption cross section is to subtract the various significant cross sections from the total cross section. These various cross sections may be calculated from empirical or theoretical approximations, giving reasonably accurate results.

Except for thermal cross sections, experimental values of the potential scattering cross section are not available for the materials used. This cross section may be approximated by the following relation in the energy range above the first resonance peak (9).

$$\sigma_p = 4\pi (R_{eff})^2$$

$R_{eff}$ is an effective radius of the nucleus, and may be obtained from Seth (11) as a function of atomic number. Seth displays a curve of the theoretical relation between $R_{eff}$ and atomic number. He also shows experimental values of $R_{eff}$ collected from even nuclei. These experimental values oscillate about the theoretical curve, showing the same general relation, even though individual data vary widely. According to Weinberg and Wigner (9), these experimental data deviate from the expected value of $R_{eff} = 1.47 \times 10^{-13} A^{1/3}$ because of the interference between potential and resonance scattering. This interference can result from single resonance peaks of "nearby" energy or it may be caused by the composite effect of many "distant" resonances. It is this latter type

of interference which causes the deviation of the experimental value for the effective nuclear radius. Because this effect is due to many "distant" resonances it is not closely dependent on the energy. Therefore the potential scattering cross section is essentially constant outside of the influence of the nearest resonance.

On the other hand, this interference between the two types of scattering must be taken into consideration since constructive interference results in an increase in the potential scattering cross section at energies above a resonance peak, and destructive interference below the resonance peak results in a lowering of the potential scattering cross section. This is adequate justification for using the smaller thermal value for the potential scattering cross section in the region below the large resonance peaks.

The resonance scattering cross section may be evaluated by the Breit-Wigner approximation

$$\sigma_{(nn)} = \pi \lambda^2 \frac{\Gamma_n \Gamma_n}{(E-E_o)^2 + (\Gamma/2)^2} = 4 \pi \lambda^2 \frac{\Gamma_n^2}{\Gamma^2}$$

which reduces to the second form at the resonance peak. Because of the interference between resonance and potential scattering it would be nearly impossible to arrive at a rigorous development of the resonance scattering cross section as a function of energy. A realistic approximation

would be to consider the area of the isosceles triangle whose height is $\sigma_{rs_{max}}$, and whose half width is $\Gamma_n$, as equivalent to the area under the resonance scattering cross section curve in the region of the resonance peak.

$$\sigma_{rs}\ (\text{area}) = \sigma_{rs_{max}} \cdot \Gamma_n = 4\pi\lambda^2 \frac{\Gamma_n^2}{\Gamma^2} \cdot \Gamma_n$$

The inelastic scattering process does not occur unless the neutron energy is higher than the first excited state of the particular material (9). Actually the inelastic scattering threshold energy is $\frac{(A+1)}{A}$ times the energy of the first excited state. The energy of this first excited state ranges from a few Mev for the smaller atomic numbers to 0.13 and 0.07 Mev for Ta and Au respectively. Thus, the inelastic scattering cross section would have to be calculated and subtracted from the total cross section in the energy range from the threshold to 2.1 Mev.

Fortunately, however, activation cross sections $\sigma_a$, are available in the higher energy ranges (6, 10). Activation cross sections are given for Au above 0.001 Mev and for Ta above 0.01 Mev. The necessary cross sections are similarly given for the other materials, and the problem of inelastic scattering is completely evaded.

Thus the activation function may be evaluated for each material over the energy ranges of interest. In order to arrive at an approximate value for the flux over the various

energy intervals, the counting rates of the various irradiated materials must be correlated to the actual disintegration rate of the foil that was caused by exposure to the flux spectrum at a particular power level.

The usual equation which relates the number of counts C recorded over a time interval $t_c$, back to the activity $A_o$ which would have been measured at the instant of removal from the reactor, a time $t_w$ before is

$$A_o = \frac{\lambda C}{(1 - e^{-\lambda t_c})(e^{-\lambda t_w})}$$

The relation between $A_o$ and the actual disintegration rate A of the foil when corrected for saturation and the various counter efficiencies that are pertinent is

$$A = \frac{A_o}{(1 - e^{-\lambda t_{ex}})(f_s)(\bar{F}_w)(W_t)(\text{power})} \quad \frac{\text{dps}}{\text{gm watt}}$$

Due to the choice of a $4\pi$ gas flow proportional counter for measuring the foil activities it is necessary to take into consideration only the self absorption factor $f_s$ and a window factor $f_w$.

The self absorption factor $f_s$ may be evaluated by the familiar equation as given in Bleuler and Goldsmith (12).

$$f_s = \frac{1}{\mu t}(1 - e^{-\mu t}) \qquad (3)$$

Absorber thickness is t and $\mu$ is the absorption coefficient. Since this relationship is valid only for gamma ray absorption, it may be adapted to beta counting only if the absorption coefficient is empirically defined in a manner such as that given by Price (13).

$$\mu = 22\, E_{max}^{-1.33} \qquad (4)$$

These empirical relationships are valid for beta particle maximum energies from 0.5 to 6 Mev, giving a good approximation for the self absorption factor. This factor becomes insensitive as it approaches unity for very thin foils. For that reason, foil weight was kept to a minimum. Experimental values have also been determined which agree with the empirical factors to within one per cent.

The window factor compensates for the fact that the beta particles which are counted by the lower electrode must travel through an aluminized mylar support film while those counted by the upper electrode have an unobstructed path. In addition to the support film of mylar, Mn, Au, In and I foils are sealed in a packet with mylar windows. Thus, for these materials, the window factor must take into consideration two thicknesses of mylar for the betas being counted in the lower hemisphere, while those beta particles being counted in the upper hemisphere go through only one thickness of mylar. The mylar used is only about 0.9 mg/sq cm thick, so that the

window factor is only a minor effect, resulting in values of the window factor which range from a low of 0.95 to a high of 0.99. The insensitivity of this factor justifies the use of the empirical approximation, relations 3 and 4. Where mylar is used only for the support, the count rate measured in the upper hemisphere is just half the disintegration rate.

$$CR_u = \frac{D}{2}$$

The count rate measured in the lower hemisphere is

$$CR_d = \frac{D}{2} f_w$$

$$\therefore CR_T = \frac{D}{2}(1 + f_w) = D\left(\frac{1 + f_w}{2}\right)$$

Similarly for the foils which are sealed in a packet with mylar windows, the factor is

$$CR_T = D\left(\frac{f_w + f_w'}{2}\right)$$

Where $f_w'$ is the factor for two thicknesses of mylar as seen by the betas going into the lower hemisphere, and $CR_T$ is the total count rate. Therefore the resultant window factor $\bar{F}_w$ is defined below depending on the foil material.

$$\bar{F}_w \equiv \left(\frac{1 + f_w}{2}\right) \quad \text{or} \quad \bar{F}_w \equiv \left(\frac{f_w + f_w'}{2}\right) \tag{5}$$

The experimental data used to calculate the actual disintegration rate has been normalized both for foil weight and

the power level of the reactor. This was necessary since the various foils were irradiated at different power levels in order to obtain adequate counting rates.

# EXPERIMENT

The experimental work divided itself quite distinctly into three categories. Total and activation cross sections were graphically or numerically integrated over the pertinent energy intervals for each foil material used. A technique of foil preparation was developed that resulted in relatively durable foils of materials that remained stable in weight, had low hazard rating and were thin enough to be acceptable beta sources. The final experimental phase was the collection of data from foils which had been irradiated in the Iowa State University UTR-10 reactor, and the computation of the resultant average flux spectrum.

The graphical integration of $G = \int_{E_1}^{E_2} \frac{\sigma_T}{E} dE$ was accomplished by plotting linear graphs of $\frac{\sigma_T}{E}$ versus E for each of the chosen materials, then integrating the area under each curve with a planimeter, excluding the large resonance peaks of indium gold and manganese.

As mentioned in the previous section, a separate integration procedure had to be used in the immediate neighborhood of large resonance peaks. When the product of the macroscopic total cross section and the thickness of the source foil exceeded 0.01, numerical integration was used (equation 2). This double integral of a function which

contained both variables was evaluated by calculating the volume enclosed by a $\Delta\mu$, a $\Delta E$, and a height represented by the function f evaluated at $(\mu_1, E_1)$ where $\mu_1$ and $E_1$ are values in the center of the $\Delta\mu$ and $\Delta E$ intervals.

The $\Delta\mu$ intervals chosen were 0.1 wide and the $\Delta E$ intervals chosen were the smallest increments compatable with the data sheets from which the cross section information was taken (6). The summation of these volumes from $\mu = 0$ to $\mu = 1$ and over the energy region of interest was used as an approximation of the cross section integral.

Cross section information used in both of these methods was obtained from Hughes and Schwartz (6) and Hughes et al. (10). The data obtained by these integrations were either total cross sections or $(n, \gamma)$ activation cross sections, and in the energy regions where the total cross section was the only information known, the cross sections due to potential scattering and resonance scattering had to be subtracted from the total cross section to obtain the desired activation cross section.

Potential scattering cross sections obtained from the relation $\sigma_p = 4\pi R_{eff}^2$ were used for the energy region above the first resonance peak, but thermal cross section values were used for the energy region below the first resonance peak. Values for $R_{eff}$ as a function of atomic number were found in Seth (11), and the values of the potential

scattering thermal cross section were given in Hughes and Schwartz (6). Since the potential scattering cross section was effectively independent of energy, the appropriate potential scattering cross section was multiplied by the logarithm of the particular energy interval to obtain $\bar{\sigma}_p$, an effective value of potential scattering over the energy interval.

$$\bar{\sigma}_p = \sigma_p \int_{E_1}^{E_2} \frac{dE}{E} = \sigma_p \ln \frac{E_2}{E_1}$$

The resonance scattering cross section also had to be subtracted from the total cross section wherever it contributed a significant portion of the total. The resonance scattering cross section was calculated from the Breit-Wigner relationship and the necessary level widths were found in Hughes and Schwartz (6). An effective value of the resonance cross section over an energy interval was obtained by summing the effective areas of the resonance cross section peaks which fall in the energy interval, then dividing by the width of the interval to obtain an effective average value. The effective areas of the resonance cross section peaks were calculated from the relation developed in the previous section.

$$\bar{\sigma}_{rs} = \frac{1}{E_2 - E_1} \sum_i \left( 4\pi \lambda_i \frac{\Gamma_{n_i}^2}{\Gamma_i^2} \right) \cdot (\Gamma_{n_i})$$

The selection of foil material was based on several considerations. The first requirement was that the naturally occurring element was isotopically pure. The reason for this was that the data given in Hughes and Schwartz (6) were listed for naturally occurring elements, however the activation cross section for a particular (n, $\gamma$) reaction was the desired information. If the naturally occurring element was 100 per cent one particular isotope, then the absorption cross section for that element would be the (n, $\gamma$) activation cross section of that isotope. Equally important requirements were that the element had to have a reasonably large cross section and a reasonably long half-life. Materials which satisfied the above conditions were Mn, Ta, Y, Co, In, Au, V, As, and I. One exception to the first requirement was In. Naturally occurring In is 95.8 per cent isotope 115 and 4.2 per cent isotope 113. However, the portion of the total cross section due to the isotope 115 was known to be 0.736 therefore the requirement of isotopic purity could be waived.

One additional factor taken into consideration was the materials hazard rating. Of the materials under consideration, As had a number one hazard rating due to its toxicity. Since only six materials were required to supply information for the calculation of an average flux in the six energy decades, As was rejected leaving eight materials.

There also appeared to be some contradiction and

uncertainty in the cross sections of Y since its potential scattering was indicated to be of a larger value than the total cross section; therefore Y was rejected leaving seven available materials. The six materials selected from these were In, Mn, Au, Ta, I, and V.

There were several available techniques for measuring the activation of irradiated materials. Two accurate methods were the use of a gamma ray scintillation detector coupled to a single channel analyzer, and the use of a gas flow proportional detector operating in the beta region.

In the first method, the scintillator collects gamma rays of all energies, produced by the decaying radioactive nuclide, however the single channel analyzer registers only those gammas occurring in a selected energy bandwidth or interval. Since gammas of a particular energy are emitted with a definite probability for each decay process, the usefulness or accuracy of this method depends on the accuracy to which the decay chain probabilities are known for the particular nuclide which has been activated. In the case of Au, In or some other thoroughly investigated element, the decay chain probabilities are very accurately known, however, for other metals such as Ta or V, the accuracy with which the decay chain probability is known may be of nearly the same order of magnitude as the probability itself. For this reason, the second method was chosen to measure the foil activation.

The second method utilized a gas flow proportional detector operating in the beta region to record the beta particles that were emitted as the activated nuclide decayed to a stable configuration. A detector with $4\pi$ geometry was utilized so that essentially all beta particles that got out of the foil volume were detected regardless of their emission direction. In such a detector, effectively all beta particles emitted are detected and less than 1 per cent of the gamma rays present are registered.

In addition to the fact that the geometry factor and the counting efficiency factor were unity, the backscattering factor was also equal to one. The window factor was very nearly unity since the support film is mylar of only 0.9 $mg/cm^2$ thickness. However since this factor could easily be calculated using the empirical relationships mentioned in the previous section, a correction was made for the effect of the mylar window on the counting rate as a function of the various energy beta particles.

The only remaining detector factor which had to be considered is the self absorption factor. This was the only important factor which must be evaluated when using the $4\pi$ gas flow proportional detector. In order to keep the self absorption factor as close to unity as possible, those materials emitting low energy beta particles were used only in the form of extremely thin foils.

This experimental requirement for thin foil sources reinforced a similar requirement expressed in the previous section on theory. The relation between neutron flux and the activation of the foils was based on the assumption that the foils were thin, i.e., the presence of a foil in the reactor would cause effectively no flux depression or distortion.

Thus foil thickness was maintained at a minimum, with an optimum thickness being that which had: 1, a self absorption factor near unity, or at least within the experimental error of 5 per cent, i.e., 0.95 or larger; 2, a foil mass which is heavy enough to be weighed within an accuracy of 5 per cent; 3, a mass large enough to be activated to at least 20,000 cpm with the neutron flux available in the UTR-10.

For most materials, this meant a thickness of about 0.0001 in or about 0.10 mg/cm$^2$. Foils ranging in weight from about 0.02 mg/cm$^2$ to about 1 mg/cm$^2$ have been produced with a vacuum deposition or "evaporator" chamber or an electroplating device. However if the evaporator or electroplating chamber is not used, the thinnest foils which could be made were about 0.0005 in thick, produced by sandwich rolling of a many layered sample. Of the metals used, three were vacuum deposited, but two were rolled. V and Ta have very high melting temperatures and very low vapor pressures, making them incompatable with the vapor deposition process. The

sixth foil I was made by two processes. A thin crystalline layer was sublimed on to a plastic film, and a thin "blotter" was used to absorb an alcohol iodine solution.

The basic problem with either electro plating or vacuum deposition was the question of the material on which to deposit or plate the metal. The backing material had to have negligible cross sections for neutron or gamma activation. This requirement was necessary because the source material and backing had to be irradiated together in a high neutron and gamma flux. Any beta activity of the backing material would unnecessarily complicate the calculation of the activity of the source material. The backing material had to be extremely thin so that the $4\pi$ geometry of the beta detector would not be disrupted by absorption of the beta particles in the backing. Since any backing no matter how thin would absorb some of the betas emitted by the activated metal, the best material would be the thinnest. An excellent backing material was a thin film of aluminized mylar, similar to the support film used in the $4\pi$ gas flow proportional counter. Because the aluminized mylar was very thin, the empirical relationships 3 and 4 were used to calculate its absorption factor.

Vacuum deposition was chosen as the method to be used for producing the thin film sources of Mn, In, and Au because aluminized mylar was better suited to the vacuum deposition

process than to electro plating techniques.

In the vacuum deposition process, Mn which had been placed on an electrode was evaporated, in a high vacuum, onto a substrate film some distance away. The electrode was a strip of Mo 0.25 inch wide by 0.01 inch thick which has been bent into the shape of a trough for the purpose of holding the Mn powder while it was heated to its vaporization temperature. The substrate mask plate, positioned about eight inches above the electrode was a 0.01 inch thick Al sheet through which several 1 $cm^2$ square holes were cut. The substrate film of aluminized mylar was positioned over the holes so that after completion of the Mn vaporization, several neat, 1 $cm^2$ square deposits of Mn were left on the mylar substrate.

It was necessary to use extreme care in the electrode temperature control, for mylar has a melting range above 140°C. Mn evaporated at a temperature of about 1300°C. in the high vacuum, however at temperatures just above that, the radiant energy from the electrode was enough to shrivel up the mylar substrate at a distance of eight inches. The use of a second piece of Al as a backing cover for the aluminized mylar also helped somewhat in conducting the heat away from the exposed 1 $cm^2$ square "targets".

After weighing these Mn foils and the mylar substrate film upon which they had been deposited, each foil was

covered by a second mylar film and sealed around the edges by a "picture frame" of Scotch tape. In this manner, the delicate mylar films were reinforced, and the Mn foil was protected from abrasion or chipping, without drastically interfering with the transmission of the beta emitted by it.

In a similar manner, foils of Au and In were prepared. Since these metals were available in sheet form, a W wire electrode was used rather than the Mo trough, resulting in less radiant energy emission.

The other element which was somewhat difficult to prepare in the form of a thin foil was I. Since it sublimed to a certain extent at room temperature and atmospheric pressure, it was necessary to seal the I into a window type packet similar to the metallic foil packets. Many attempts were made to produce uniform deposits of I by evaporating various I solutions or compounds. These were not successful because the low surface tension of the solvents allowed the I solution to flow over the surface of the film combining with the Scotch tape edging. Next an effort was made to sublime the I, causing recrystallization of the I into 1 $cm^2$ square foils on aluminized mylar substrate films as had been accomplished with a substrate mask plate for Mn foils.

This process appeared to be somewhat questionable, however, since it produced irregular crystal formation as well as an apparent condensation of moisture on both the

aluminized mylar and the Al substrate mask plate. It was decided that this peculiar result was due to the chemical action of I on Al. The deposit was probably $AlI_3$ containing I in unknown proportions. The liquid was due to the deliquescent nature of $AlI_3$ and was probably a solution of $AlI_3 \cdot 6H_2O$.

The successful sublimation of I onto a film backing was achieved however, by using an acrilic plastic coated substrate mask plate, and an unaluminized plastic film for the substrate material. Saran Wrap was used for this purpose because it is nearly the same thickness as the mylar film.

Due to the difficulty encountered in this preparation, a set of foils was also produced by using a very thin filter paper to hold a solution of I in alcohol until the alcohol evaporated. One $cm^2$ pieces of this I laden blotter were then used for the sixth thin foil, neutron activated, source of beta particles.

The third phase of the experimental work was the collection of data and the calculation of the factors, parameters and constants necessary for the ultimate compilation of the six activation equations in terms of the six flux decades.

Of the two detector factors, the window factor was calculated from the empirical relations 5 developed in the previous section. This factor has been evaluated for each

foil, since the factor is dependent on the energy of the emitted beta particle.

The second detection factor which had to be evaluated is the self absorption factor. For most commercially available metallic foils, usually one mill or greater in thickness, the self absorption factor would be about 0.5 or even less. The most accurate method of evaluating self absorption factors of this order of magnitude was an experimental analysis. This was accomplished for all six foil materials by measuring the activation per gram for vapor deposited foils as well as commercial thickness foils.

Several identically sized foils of a given element were irradiated, then the count rate was measured for a single foil, a stack of two foils, a stack of three foils, etc. The count rate per unit weight was calculated for each group and a graph of the count rate per unit weight as a function of the weight of the foil stack was compiled. The curve was extrapolated to zero weight, then the ratio of the count rate at zero weight to the count rate per gram at the source foil weight gave a good experimental value of the self absorption factor.

These graphs are available in the monthly progress reports for 1962 of the Nuclear Engineering Department's research project, "Ten foil flux measurement project". The graph for Ta is also found in the Appendix.

The accuracy of an experimental self absorption factor is only as good as the measurement of the activity per gram of the thinnest foils, for the activity of those foils for which self absorption becomes negligible will effectively determine the activity per gram of zero thickness foils. Thus if foils can be prepared for which self absorption is almost negligible, then the experimental factor is no longer necessary, and the more direct calculation of the self absorption factor is used.

For thin foils, the self absorption factor became quite insensitive. For example, the factors corresponding to Au of thickness 0.000085 gm/cm$^2$ and 0.000215 gm/cm$^2$ were 0.999 and 0.998 respectively. Hence any error present in this factor was insignificant compared to the known inaccuracy of five per cent for the cross section data.

Of the six foil materials used, five were successfully produced as thin foils. The self absorption factors calculated for these ranged from 0.974 to 0.999 and are found in the Appendix. Since vapor deposited foils of Ta could not be satisfactorily formed, that self absorption factor was determined both experimentally and empirically. The values, 0.558 and 0.551 respectively, agree well for the averaged foil thickness of 0.0249 gm/cm$^2$.

The only remaining data to be collected are the actual activation information on each of the elements. Calculations

were made for each foil to decide on the length of the irradiation exposure and the optimum reactor power level to obtain count rates for the $4\pi$ gas flow proportional counter in the range between 20,000 and 80,000 cpm. The foils were irradiated by taping them to the forward end of the pneumatic rabbit, then after the reactor was brought up to power the pneumatic rabbit was remotely positioned next to the north core tank. Data averaged from at least five experimental values of the foil activation for each element was used in the final set of six equations in six unknowns. These data are found in the Appendix.

In order to complete the description of the neutron flux, the thermal neutron flux and the fast neutron flux were also calculated. Standard procedures were used to find these values (14). Values of the thermal and fast flux were multiplied by appropriate cross sections, and are included in the six equations in six unknowns in the form of a constant. This is necessary since each of the equations is a statement of the experimental fact that the total activation of a particular foil is the sum of the activation due to thermal neutrons, fast neutrons, and each of the six intermediate energy groups.

The thermal flux was calculated from data collected from bare and Cd covered Au foils, using the same $4\pi$ gas flow proportional detector as was used for the other source foils.

The fast neutron flux was obtained from the comparison

of the activity caused by threshold activation of Al with the activity resulting from thermal neutron activation of Al. The reaction responsible for threshold activation is $Al^{27}$ (n,p) $Mg^{27}$. Since the threshold energy is 2.1 Mev, this activation is used to calculate the neutron flux in the energy range between 2.1 Mev and the maximum fission energy.

Thermal neutrons also activate Al by the reaction $Al^{27}$ (n, $\gamma$) $Al^{28}$ and the equation showing the level of the saturated activation due to thermal neutrons is

$$A_{th}sat = K_{geom} f_{th} \Phi_{th} \sigma_{th} N = CPM_{th} (1 - e^{-\lambda_{th} t})^{-1}$$

Similarly the saturated activity of the threshold reaction due to fast neutron flux above 2.1 Mev is

$$A_f sat = K_{geom} f_f \Phi_f \sigma_f N = CPM_f (1 - e^{-\lambda_f t})^{-1}$$

Therefore the fast flux is a function of the thermal flux, the saturated activities, the detector efficiencies, and the cross sections of the two reactions.

$$\therefore \Phi_f = \Phi_{th} \frac{CPM_f}{(1 - e^{-\lambda_f t}) f_f \sigma_f} \times \frac{(1 - e^{-\lambda_{th} t}) f_{th} \sigma_{th}}{CPM_{th}}$$

Since the thermal flux has already been measured by the gold foil technique, and the other parameters are known, the fast flux may be readily calculated. The necessary data were collected with a gamma sensitive scintillation detector

coupled to a single channel analyzer. The thermal reaction results in a 1.78 Mev gamma of 2.3 min half life. This activity was measured first. Then the activity due to the threshold reaction, 0.83 Mev gamma of 9.5 min half life, was measured. The cross sections were obtained from the literature, and the scintillation crystal efficiencies for gammas of these two energies were obtained from the scintillation crystal manufactor's literature.

Thus for a known thermal flux, the fast flux is easily found from the Al threshold reaction. The six equations containing the six unknown average fluxes may now be completed with the activity contributed by the thermal and the fast flux being consolidated into the constant in each equation. The completed set of equations is then solved for the neutron flux in each of the six energy decade intervals.

The total activation is equal to the sum of the activation due to thermal flux, the activation due to the flux in each of the six energy decades, and the activation due to the fast flux, respectively. The equations are

$$\text{Au: } 2.992\times10^{6} = 2.066\times10^{6} + 1.244\Phi_1 + 1.615\times10^{-2}\Phi_2 + 8.232\times10^{-2}\Phi_3 + 1.974\times10^{-2}\Phi_4 + 5.939\times10^{-3}\Phi_5 + 1.872\times10^{-3}\Phi_6 + 7.397\times10^{2}$$

$$\text{Mn: } 1.059\times10^{6} = 1.028\times10^{6} + 5.562\times10^{-2}\Phi_1 + 2.746\times10^{-2}\Phi_2 + 3.111\Phi_3 + 1.599\Phi_4 + 1.019\times10^{-3}\Phi_5 + 2.499\times10^{-4}\Phi_6 + 9.198\times10$$

$$\text{In: } 9.975\times10^{6} = 5.728\times10^{6} + 1.208\phi_1 + 1.118\times10^{-1}\phi_2 + 2.870\times10^{-2}\phi_3$$
$$+ 2.424\times10^{-2}\phi_4 + 1.073\times10^{-2}\phi_5 + 3.295\times10^{-3}\phi_6 + 2.087\times10^{3}$$

$$\text{Ta: } 7.320\times10^{5} = 4.453\times10^{5} + 1.746\phi_1 + 1.299\phi_2 + 1.419\times10^{-1}\phi_3$$
$$+ 3.319\times10^{-2}\phi_4 + 7.357\times10^{-3}\phi_5 + 2.224\times10^{-3}\phi_6 + 8.982\times10^{2}$$

$$\text{V: } 4.415\times10^{5} = 3.745\times10^{5} + 1.726\times10^{-1}\phi_1 + 1.182\times10^{-1}\phi_2 + 1.623\phi_3$$
$$+ 9.398\times10^{-1}\phi_4 + 4.686\times10^{-1}\phi_5 + 1.178\times10^{-4}\phi_6 + 5.071\times10$$

$$\text{I: } 3.973\times10^{5} = 1.869\times10^{5} + 1.571\times10^{-2}\phi_1 + 8.948\times10^{-1}\phi_2 + 1.209\times10^{-1}\phi_3$$
$$+ 2.492\times10^{-2}\phi_4 + 8.696\times10^{-3}\phi_5 + 2.170\times10^{-3}\phi_6 + 7.885\times10^{2}$$

# RESULTS

The solutions to the six equations are surprising. The flux in the energy interval from 0.4-10 ev is positive, but that in the intervals from 10-100 ev, 100-1000 ev and 0.01-0.1 Mev is negative. The flux in the remaining two intervals is also positive.

Because these solutions are closely interrelated by the six simultaneous equations, no significance can be attached to either the sign, or the numerical value of any of the flux values.

Thus it is concluded that even though the following values of the flux have been calculated, they are either incorrect, or the unknown "error flags" associated with these average values of the flux are larger than their respective absolute values.

$\bar{\Phi}_1$(0.4-10 ev) = $1.029 \times 10^5$

$\bar{\Phi}_2$(10-100 ev) = $-9.179 \times 10^4$

$\bar{\Phi}_3$(100-1000 ev) = $-2.848 \times 10^7$

$\bar{\Phi}_4$(1000-10000 ev) = $5.525 \times 10^7$

$\bar{\Phi}_5$(10000-100000 ev) = $-1.233 \times 10^7$

$\bar{\Phi}_6$(0.1-2.1 Mev) = $1.136 \times 10^9$

# CONCLUSIONS

The question which has subsequently arisen is "Why doesn't the solution represent a reasonable flux spectrum?" Certainly, the computer can only produce a solution to the equations which were supplied. This has been done correctly, for substitution of the values for the flux into the equations satisfies them. Thus it must be concluded that a source of error is present which results in inexact or incorrect components of the activation equations.

During the course of this research problem, many errors of both known and unknown extent made themselves apparent. Since the activation equations were first solved, yielding partially positive and partially negative values, a continuous effort has been made to refine all constants, coefficients and terms down to errors much less than five per cent. Five per cent is really the accuracy limit of the experiment since it is the accuracy limit on cross section data, and at least one cross section is found in every term of each activation equation. As a result, three areas of unknown inaccuracy came under closer scrutiny. They were the purity of foil materials used, the self absorption factor and the potential scattering cross section.

Foil purity was verified by two methods, half life measurement, and spectrographic analysis. All half life

measurements agreed with the published values within one per cent (15). This indicates that any activation of a foil is due to the desired element and/or an impurity with very nearly the same half life. Spectrographic analysis shows what impurities are present, and to what extent. Thus a correction can be made for activation caused by any impurity which may have had a very similar half life. The only significant impurities in the Au used were Ag-500 ppm, Pd-500 ppm, Pt-500 ppm, and Cu-100 ppm. The impurity with the most similar half life is $Pt^{197}$. The ratio of this Pt half life to the half life of $Au^{198}$ is 0.75/2.70 or 0.278. The significant impurities in I were Ta-500 ppm, Si-100 ppm, Ni-100 ppm, Fe-200 ppm, Cu-100 ppm, Cr-100 ppm. The stable isotope which could cause the most similar half life is $Cu^{66}$. The ratio of the half lives of $Cu^{67}$ to $I^{128}$ is 5.1/25.0 or 0.204. The impurities present in V are Ca-100 ppm, Fe-100 ppm and Si-100 ppm. Of these, $Ca^{49}$ most closely resembles the half life of V with a half life ratio of 8.5/2.3 or 3.70. The impurities found in Ta are Cu-100 ppm, Fe-100 ppm, Nb-200 ppm, Mg-100 ppm, and Si-100 ppm. $Fe^{58}$ has a half life compared to the half life of Ta of 45.1/115 or 0.40. Mn has 100 ppm of Cu and 100 ppm Mg in it as impurities. The ratio of the half lives for $Cu^{63}$ and Mn is 12.8/2.58 or 4.96. Indium is the last of the materials, and has the following impurities: Al-100 ppm, Ca-100 ppm, Cu-100 ppm, Fe-100 ppm, Ni-100 ppm and Si-100 ppm. The

isotope with a half life closest to that of $In^{116}$ is $Cu^{67}$. The ratio of these half lives is 54/5.1 or 10.6.

Since none of the impurities have half lives close enough to the half life of the major constituent to provide activation which would not be detected as an incorrect half life measurement, it is concluded that the activation measured in the half life measurements and in the data collection measurements was actually due to the activation of the major constituent of the foil and not due to any impurity.

The second area of possible error which has been eliminated is that of the self absorption factor. Early solutions of the activation equations were based on experimental values of the self absorption factor which had been determined with commercial thickness foils. These factors differed considerably from values obtained with the empirical relationships. This problem arises from the experimental procedure whereby the activation per gram must be extrapolated to zero thickness using data from relatively thick foils. The problem was avoided in the final solution of the activation equations, by using thin foils and the empirical self absorption relationships which are then valid. The only exception to this procedure was the method used for Ta, since thin Ta foils could not be satisfactorily produced. Fortunately however, the experimental and empirical methods agreed closely for the value of the factor for Ta. An average of the two was used

for the activation calculation.

The potential scattering cross sections are a third area of extensive but undetermined error. There is no direct proof that the error found in these cross sections is responsible for the answers given by the activation equations, and for that matter there is no direct proof that there is error present in the particular cross sections that have been used in the activation equations. However the demonstration of a gross contradiction in the cross sections published for other materials must lead to the conclusion that since all other errors possible have been held or reduced to a reasonable minimum, the failure of the activation equations to yield credible values for the flux is attributable to an undetermined amount of error in the potential scattering cross section values.

In the theory section, the problem of interference between resonance and potential scattering was briefly discussed. Based on the physical interpretation of constructive and destructive interference, it was assumed that the potential scattering cross section below the first large resonance peak could be best approximated by the published thermal value of potential scattering. However in the energy region above resonance it was assumed that potential scattering cross sections calculated from the effective nuclear radius should be used, resulting in generally larger values, due

supposedly to constructive interference.

If these assumptions are valid, then, for a material which has no resonance peaks, such as Y, the thermal value should correspond very closely to the value calculated from the effective nuclear radius. In fact however, they differ by 110 per cent. The value of the potential scattering cross section calculated from the nuclear raidus is even larger than the total cross section in the energy range from 0.1 to 1 mev. Y was rejected as a foil material because of this discrepancy. Since the cross section calculated from the effective radius is in disagreement with two independent, experimentally measured cross sections, it must be concluded that the effective nuclear radius is incorrect.

It would be desirable to compare these values of the potential scattering for the foil materials which have been used. Unfortunately, all of these elements have resonance peaks, so that the thermal value for potential scattering would not be expected to correspond to the value obtained from the effective nuclear radius, and no comparison is possible.

However, the value of the nuclear radius is obtained from a graph of experimental values of the effective radius for even Z nuclei. Therefore, an element of doubt is thrown on all values of the potential scattering cross section calculated from the effective nuclear radius, since all of

the foil materials, including Y, are odd Z elements.

This would indicate that even though the use of these potential scattering cross sections may not introduce an error of 110 per cent as happened for Y, an error of significant but undetermined size has been introduced. Since all other errors have been minimized, this is the only known source of error which could be responsible for the failure of this flux measurement.

## LITERATURE CITED


1. Zinn, W. H. The Bragg reflection of neutrons by a single crystal. Physical Review 70: 102. 1946.

2. Hughes, D. J. Pile neutron research. Cambridge, Mass., Addison-Wesley Publishing Co., Inc. 1953.

3. Fischer, G. J. Neutron energy spectrum measurements in unmoderated assemblies. Nuclear Science and Engineering. 7: 355-362. 1960.

4. Grader, R. J. Measuring reactor neutron spectra with threshold detectors. U. S. Atomic Energy Commission Report UCRL-6089 (California. Univ., Livermore. Radiation Lab.). 1960.

5. Pai, H. L., Ma, P. Y., Wang, S. C. and Lee, W. S. Measurement of epithermal neutron spectra by resonance detectors. Nuclear Science and Engineering. 9: 519-520. Apr. 1961.

6. Hughes, D. J. and Schwartz, R. B. Neutron cross sections. U. S. Atomic Energy Commission Report BNL-325 (Brookhaven National Lab., Upton, N. Y.). 1958.

7. Jablonski, F. E. and DiMeglio, A. F. Use of aluminum as a threshold neutron detector. Nuclear Science and Engineering. 3: 631-633. March, 1958.

8. Hwang, R. N. Neutron energy spectrum; nuclear engineering internal project report. (Manuscript) Ames, Iowa, Nuclear Engineering Dept., Iowa State University of Science and Technology. Feb. 16, 1961.

9. Weinberg, A. M. and Wigner, E. P. The physical theory of neutron chain reactors. Chicago, Ill., The University of Chicago Press. 1958.

10. Hughes, D. J., Magurno, B. A. and Brussel, M. K., Neutron cross sections. U. S. Atomic Energy Commission Report BNL-325 (Brookhaven National Lab., Upton, N. Y.). Supplement 1. 1960.

11. Seth, K. K. Nuclear size by potential-scattering cross sections. Conference on neutron physics by time-of-flight. U. S. Atomic Energy Commission Report ORNL-2309 (Oak Ridge National Lab., Tenn.). November 1, 1956.

12. Bleuler, E. and Goldsmith, G. J. Experimental nucleonics. New York, N. Y., Rinehart and Co., Inc. 1952.

13. Price, W. J. Nuclear radiation detection. New York, N. Y., McGraw-Hill Book Co., Inc. 1958.

14. Greenfield, M. A., Koontz, R. L. and Jarrett, A. A. Absolute thermal neutron determination. Part 1. U. S. Atomic Energy Commission Report NAA-SR-1137 (North American Aviation, Inc., Downey, Calif.). December 1, 1955.

15. Strominger, D., Hollander, J. H., and Seaborg, G. T. Table of Isotopes. Reviews of Modern Physics 30: 585-904. 1958.

ACKNOWLEDGMENTS

The author expresses sincere gratitude to Dr. Glenn Murphy, Head of the Department of Nuclear Engineering, not only for his suggestions, encouragement, and criticism during the experiment and preparation of this thesis, but also for providing the research project under which the experiment was performed.

A debt of gratitude is also owed to Dr. D. D. Glower and Mr. R. N. Hwang who introduced the problem to the author and gave immeasurable assistance through the ensuing discussions with the author.

Finally, the author extends his appreciation to all those members of the Iowa State University staff who have offered assistance and suggestions during the various phases of the experiment and the evaluation of its results.

# APPENDIX

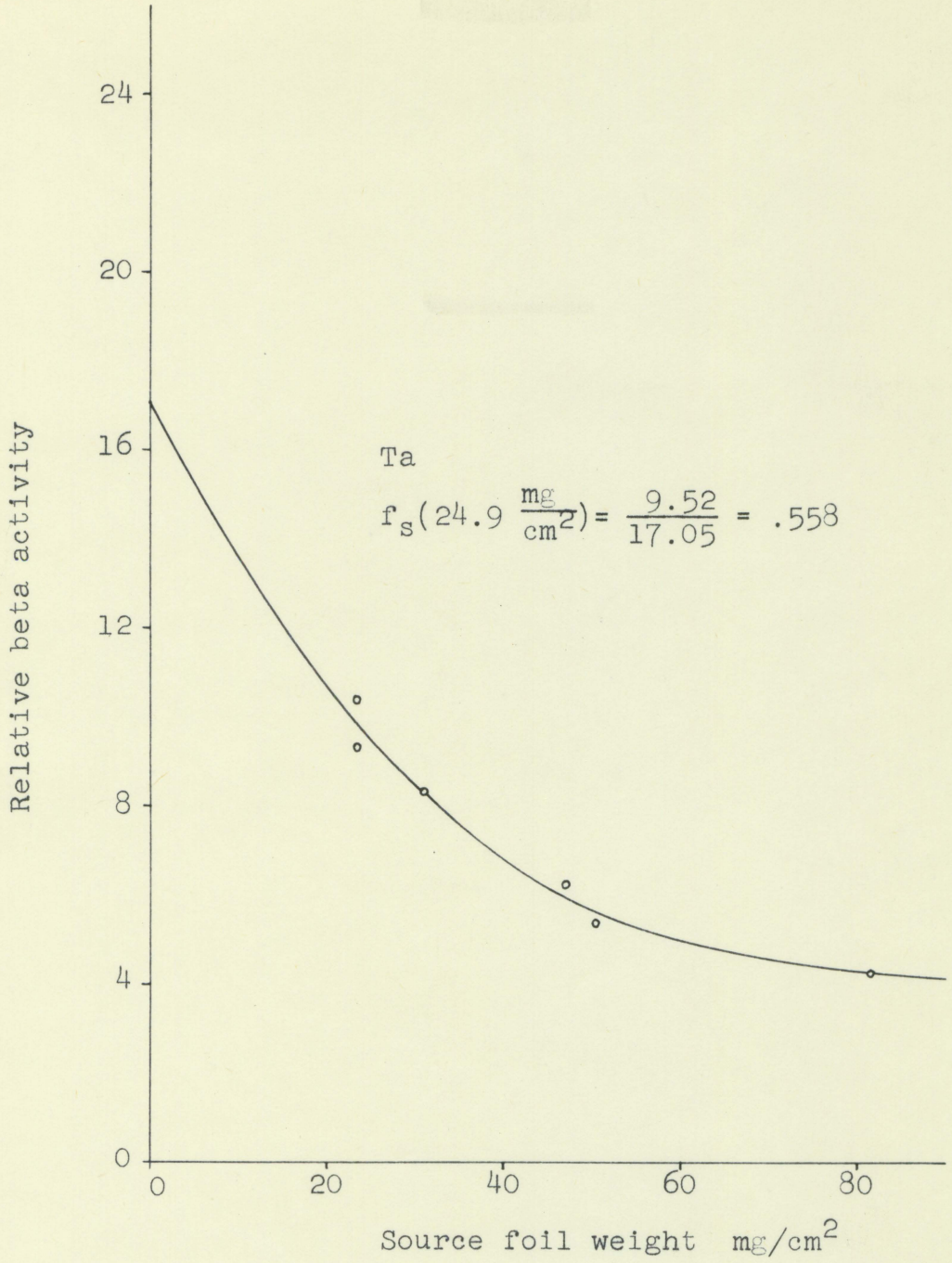


Fig. 1. Data for experimental self absorption factors

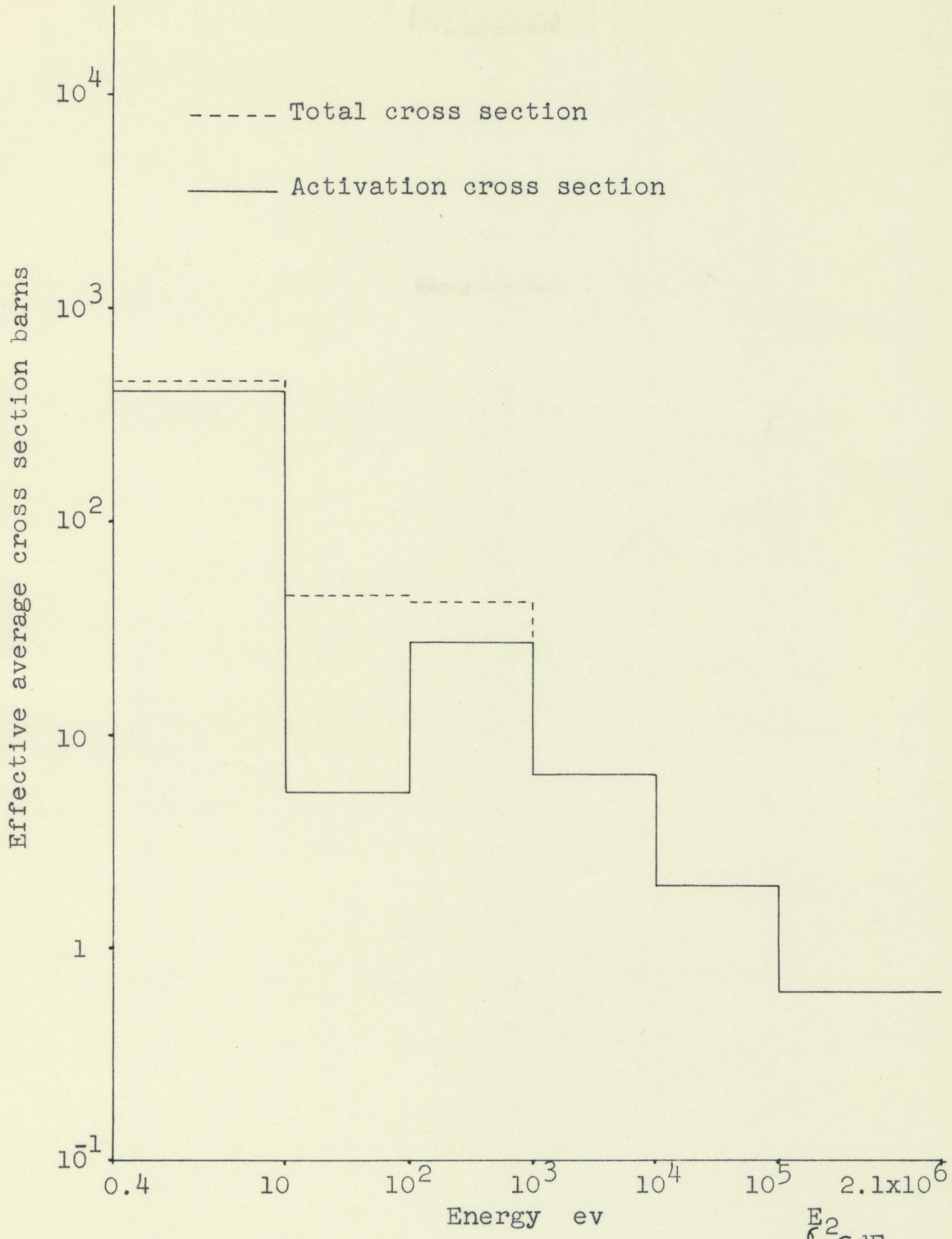


Fig. 2. Effective average cross sections for Au $\int_{E_1}^{E_2} \frac{\sigma\, dE}{E}$

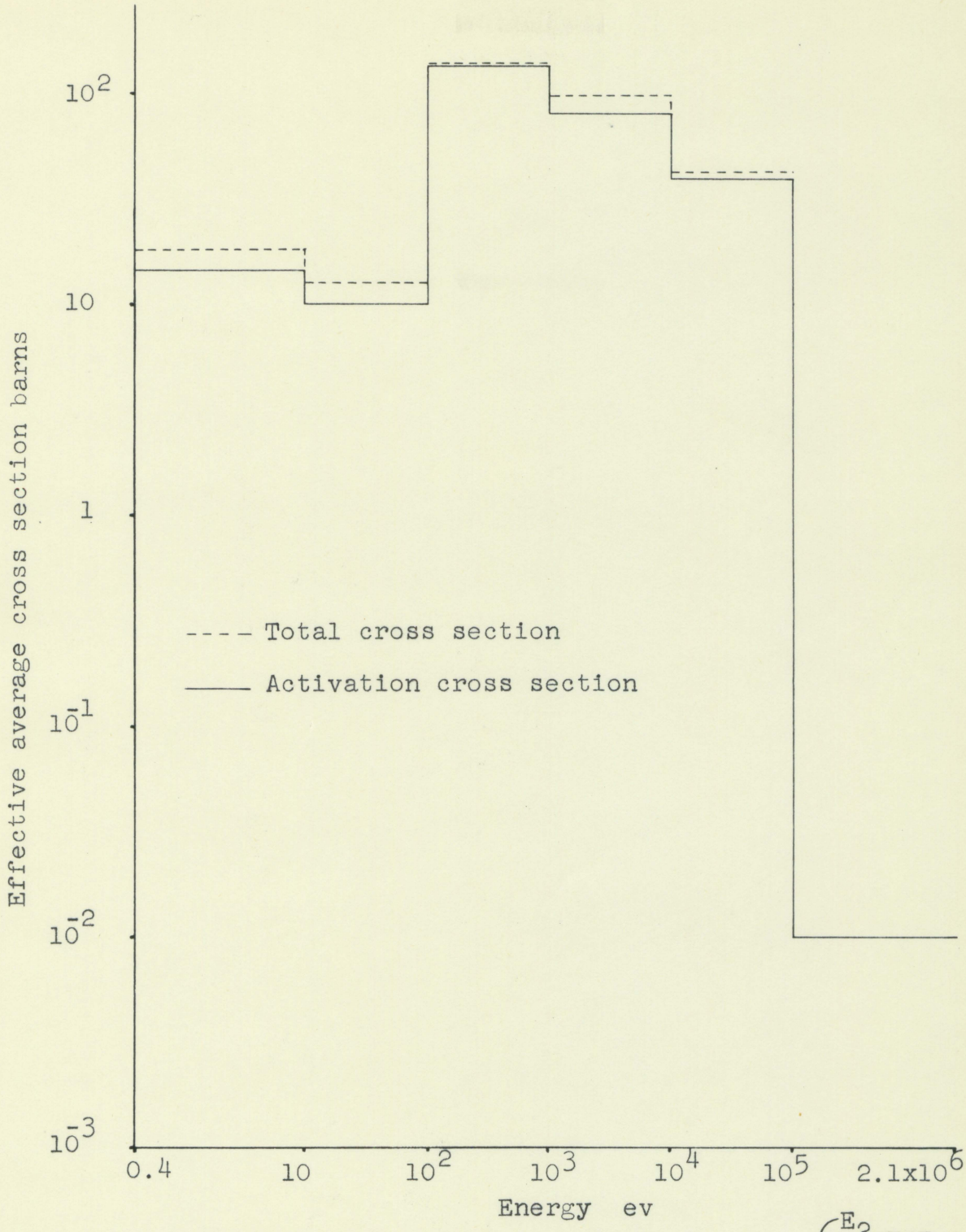


Fig. 3. Effective average cross sections for $V \int_{E_1}^{E_2} \frac{\sigma dE}{E}$

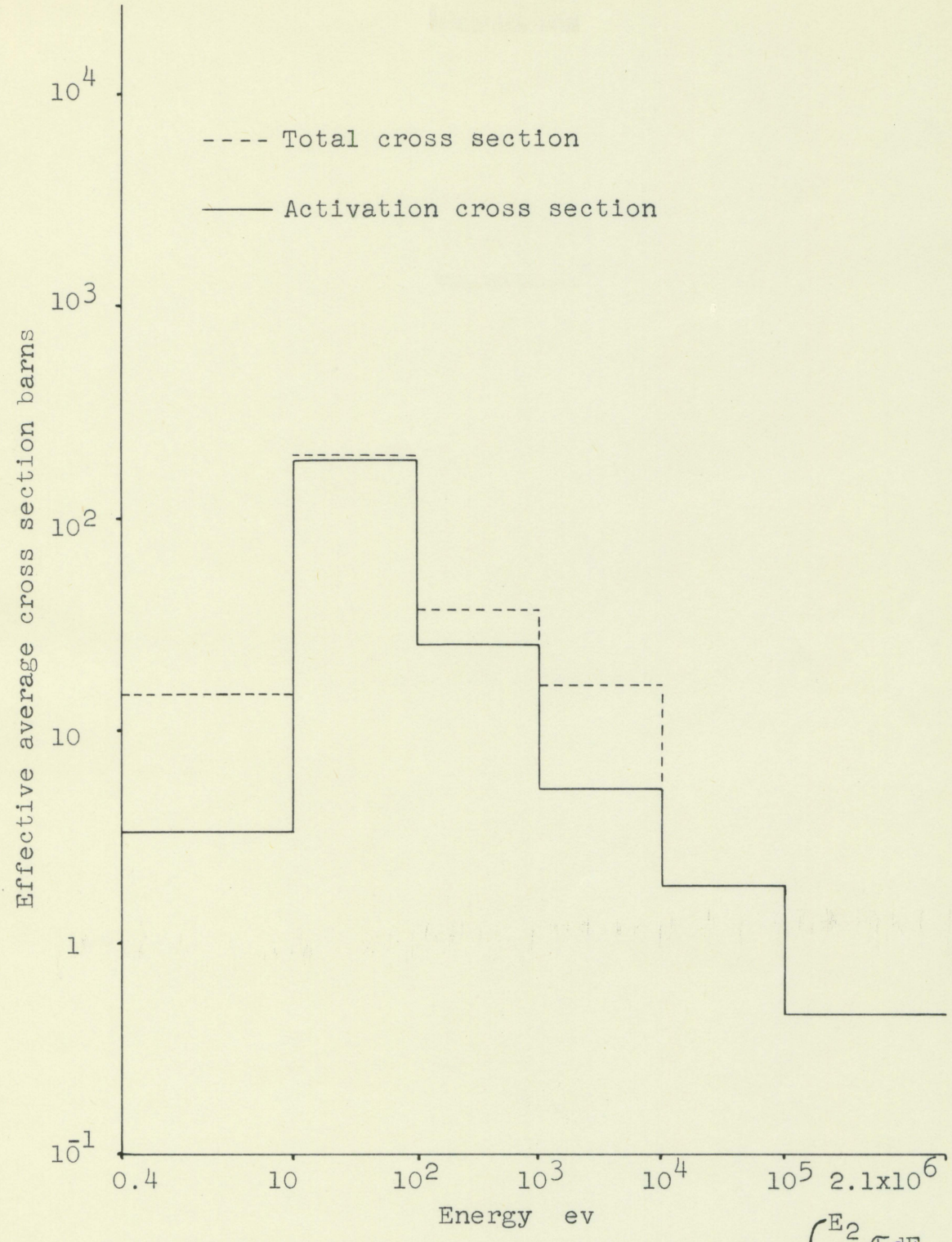


Fig. 4. Effective average cross sections for $I \int_{E_1}^{E_2} \frac{\sigma dE}{E}$

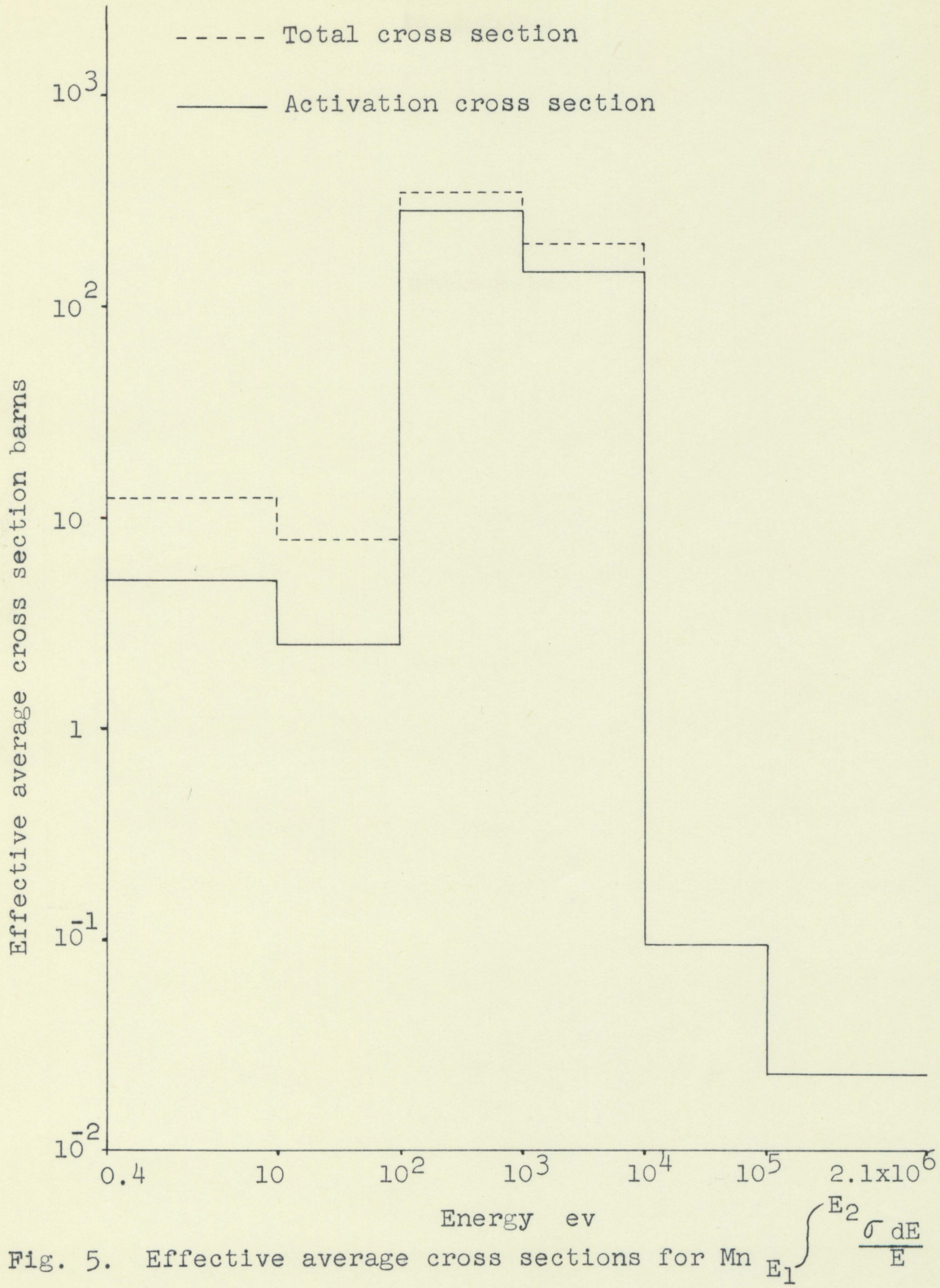


Fig. 5. Effective average cross sections for Mn $\int_{E_1}^{E_2} \frac{\sigma \, dE}{E}$

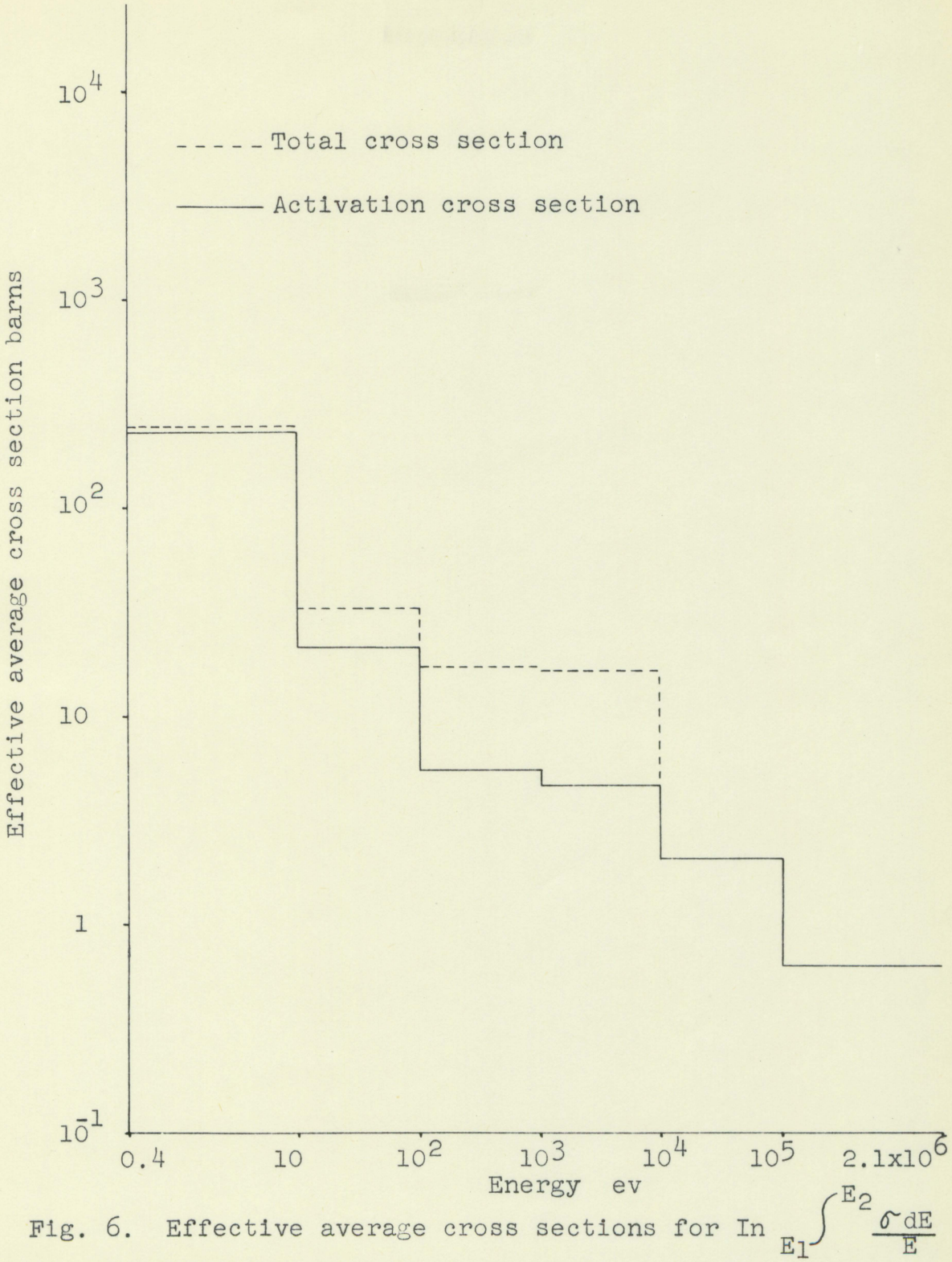


Fig. 6. Effective average cross sections for In $\int_{E_1}^{E_2} \frac{\sigma \, dE}{E}$

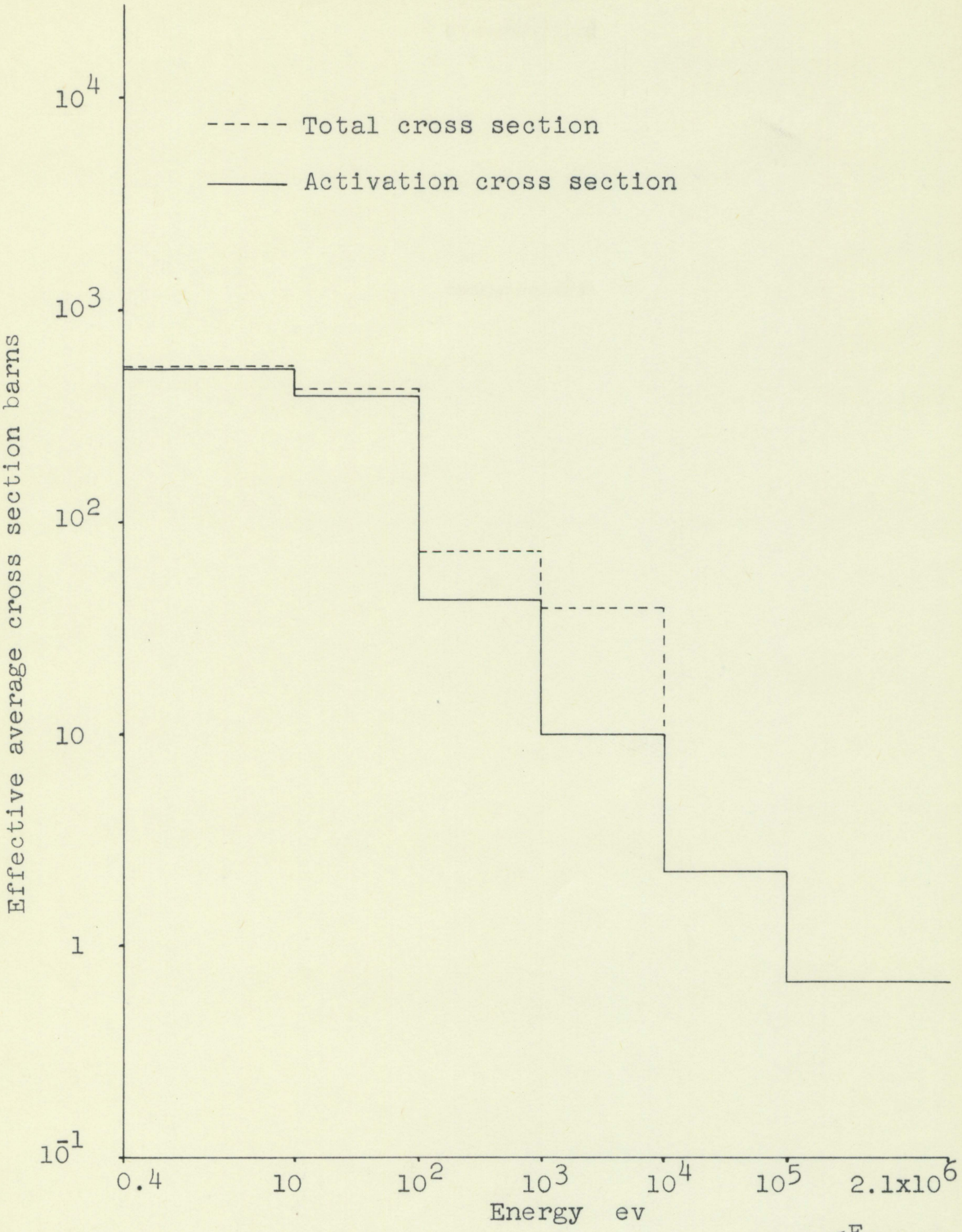


Fig. 7. Effective average cross sections for Ta $\int_{E_1}^{E_2} \frac{\sigma \, dE}{E}$

## Relations Used to Calculate True Disintegration Rate of Foil Material

$D(\frac{dps}{gm\ w})$ is the true disintegration rate of a foil material per gram of weight and watt of reactor power.

$$D = \frac{A_o ave}{60\ sec/min\ f_s \times f_w\ P} \times \frac{1}{(1 - e^{-\lambda t_{ex}})}$$

$$A_o = \frac{\lambda C_{net}}{(1 - e^{-\lambda t_c})(e^{-\lambda t_w})}$$

$A_o$ is the activation of a foil per gram of weight at the instant of removal from the reactor.

$A_o ave$ is the average $A_o$ calculated from the activation data.

$C_{net}$ is the total net count collected in the time interval $t_c$.

$t_c$ is the interval of counting time.

$t_w$ is the interval of waiting time between removal from the reactor and begin of count.

$t_{ex}$ is the exposure time in the reactor flux.

P is the power level of the reactor in watts during exposure.

$f_s$ is the self absorption factor.

$f_w$ is the window absorption factor.

| | Material | | | | | |
|---|---|---|---|---|---|---|
| | I | In | Mn | V | Ta | Au |
| $A_o ave\ x(10^{-6})$ | 56.43 | 1374. | 26.64 | 21.26 | 0.995 | 623. |
| P | 10 | 20 | 10 | 1 | $10^3$ | $2x10^2$ |
| $f_s \times F_w$ | 0.976 | 0.953 | 0.9445 | 0.955 | 0.545 | 0.975 |
| $D\ x\ (10^{-5})$ | 3.973 | 99.75 | 10.59 | 4.415 | 7.320 | 29.92 |

## Relations Used to Calculate Self and Window Absorption Factors

$$f_s = \frac{(1-e^{-\mu t})}{\mu t} \qquad \bar{F}_w = \frac{1}{2}\left[\frac{(1-e^{-\mu t'})}{\mu t'} + \frac{(1-e^{-\mu t''})}{\mu t''}\right] \qquad \mu = \frac{22}{E_m^{1.33}}$$

$f_s$ is the self absorption factor.

t is the average thickness of the group of activation foils.

$f_w$ is the average window absorption factor.

t' is the thickness of the upper packet window.

t" is the thickness of the lower window.

$\mu$ is an empirical absorption coefficient.

$E_m$ is the maximum energy of the beta particle.

| | Material | | | | | |
|---|---|---|---|---|---|---|
| | I | In | Mn | V | Ta* | Au |
| $E_m$(Mev) | 1.67 | 0.60 | 0.75 | 2.60 | 0.51 | 0.96 |
| $\mu$ | 11.12 | 43.51 | 32.26 | 6.176 | 53.86 | 23.23 |
| t ($gm/cm^2$) x ($10^4$) | 3.13 | 0.983 | 14.2 | 134. | 249. | 1.02 |
| t' ($gm/cm^2$) x ($10^3$) | 2.87 | 1.4 | 1.4 | -- | -- | 1.4 |
| t" ($gm/cm^2$) x ($10^3$) | 4.27 | 2.8 | 2.8 | 1.4 | 1.4 | 2.8 |
| $\bar{F}_w$ | 0.977 | 0.955 | 0.966 | 0.998 | 0.982 | 0.976 |
| $f_s$ | 0.999 | 0.998 | 0.978 | 0.957 | 0.551 | 0.999 |

*Experimental $f_s$ = 0.558

Ave $f_s$ = 0.555

## Ta Activation Data

Activated Aug. 18, 1961 1426-1436 Hr 1.0 kw Run 286
*Feb. 12, 1962 1620-1630 Hr 2.0 kw Run 349

| Foil no. | Wt.(gm) | Gross CPM | Bkgd | Std. dev. | Time |
|---|---|---|---|---|---|
| Ta 23 | 0.0236 | 11,030 | 135 | 105 | Jan. 3, 1962 |
| Ta 24 | 0.0235 | 9,976 | 135 | 99 | Jan. 3, 1962 |
| Ta 21* | 0.0275 | 47,192 | 108 | 217 | Mar. 7, 1962 |
| Ta 23 | 0.0236 | 10,432 | 134 | 102 | Jan. 13, 1962 |
| Ta 24 | 0.0235 | 9,589 | 134 | 97 | Jan. 13, 1962 |
| Ta 21* | 0.0275 | 39,596 | 207 | 199 | Apr. 3, 1962 |

## Self Absorption Data

Activated Aug. 18, 1961 1426-1436 Hr 1.0 kw Run 286

| Foil no. | Wt.(gm) | Gross CPM | Bkgd | Std. dev. | Time |
|---|---|---|---|---|---|
| Ta 22 | 0.0235 | 23,102 | 93 | 152 | Aug. 20, 1961 |
| Ta 23 | 0.0236 | 24,450 | 93 | 157 | Aug. 20, 1961 |
| Ta 24 | 0.0235 | 21,895 | 93 | 148 | Aug. 20, 1961 |
| Ta 25 | 0.0308 | 25,486 | 93 | 160 | Aug. 20, 1961 |
| Ta 26 | 0.0506 | 27,020 | 93 | 164 | Aug. 20, 1961 |
| Ta 28 | 0.0471 | 29,431 | 93 | 172 | Aug. 20, 1961 |
| Ta 29 | 0.0814 | 34,480 | 93 | 186 | Aug. 20, 1961 |

## Mn Activation Data

Activated Aug. 18, 1961 1444-1454 Hr 10 w Run 286

| Foil no. | Wt.(gm) | Gross CPM | Bkgd | Std. dev. | Time (hr) |
|---|---|---|---|---|---|
| Mn 32 | 0.00155 | 29,476 | 115 | 172 | 1609 |
| Mn 33 | 0.00118 | 21,346 | 115 | 146 | 1615 |
| Mn 34 | 0.00130 | 23,804 | 115 | 154 | 1621 |
| Mn 35 | 0.00165 | 30,639 | 115 | 175 | 1626 |
| Mn 36 | 0.00140 | 24,343 | 115 | 156 | 1631 |

## I Activation Data

Activated Mar. 15, 1962 1128-1138 Hr 10 w Run 359

| Foil no. | Wt.(gm) | Gross CPM | Bkgd* | Std. dev. | Time (min) |
|---|---|---|---|---|---|
| I 1 | 0.00029 | 11,001 | 283 | 104 | 1150.33 |
| I 2 | 0.000345 | 11,267 | 210 | 105 | 1156.15 |
| I 3 | 0.000305 | 9,150 | 181 | 95 | 1162 |
| I 1 | 0.00029 | 5,803 | 153 | 75 | 1174 |
| I 2 | 0.000345 | 5,888 | 145 | 76 | 1180 |
| I 3 | 0.000305 | 4,702 | 133 | 68 | 1186 |

*Background value includes a correction for activation of a blank packet as a control.

## V Activation Data

Activated Mar. 27, 1962 1028-1038 Hr 1 w Run 366

| Foil no. | Wt.(gm) | Gross CPM | Bkgd | Std. dev. | Time (hr) |
|---|---|---|---|---|---|
| V 20 | 0.0106 | 100,833 | 195 | 318 | 1042 |
| V 22 | 0.0116 | 52,698 | 195 | 230 | 1046 |
| V 25 | 0.0180 | 22,323 | 195 | 149 | 1053 |
| V 20 | 0.0106 | 7,657 | 195 | 86 | 1056 |
| V 22 | 0.0116 | 4,067 | 195 | 62 | 1100 |
| V 25 | 0.0180 | 1,894 | 195 | 41 | 1107 |

## In Activation Data

Activated Mar. 22, 1962 1201-1211 Hr 20 w Run 364

| Foil no. | Wt.(gm) | Gross CPM | Bkgd* | Std. dev. | Time (hr) |
|---|---|---|---|---|---|
| In 7 | 0.000075 | 94,504 | 664 | 306 | 1220 |
| In 8 | 0.000105 | 113,762 | 195 | 337 | 1226 |
| In 9 | 0.000115 | 118,496 | 166 | 344 | 1232 |
| In 7 | 0.000075 | 45,808 | 128 | 214 | 1316 |
| In 8 | 0.000105 | 56,408 | 126 | 238 | 1321 |
| In 9 | 0.000115 | 59,616 | 125 | 244 | 1326 |

*Background value includes correction for activation of control packet.

## Au Activation Data

Activated Jul. 14, 1961 1500-1510 Hr 10 w Run 267

| Foil no. | Wt.(gm) | Gross CPM | Bkgd | Std. dev. | Time |
|---|---|---|---|---|---|
| Au 1* | 0.0613 | 20,893 | 522 | 145 | 1515 Jul. 14, 1961 |
| Au 1* | 0.0613 | 12,547 | 201 | 111 | 1405 Jul. 16, 1961 |

Activated Apr. 4, 1962 1125-1135 Hr 200 w Run 375

| Foil no. | Wt.(gm) | Gross CPM | Bkgd | Std. dev. | Time |
|---|---|---|---|---|---|
| Au 14 | 0.000090 | 55,549 | 128 | 236 | 1145 Apr. 4, 1962 |
| Au 15 | 0.000105 | 65,751 | 128 | 256 | 1150 Apr. 4, 1962 |
| Au 16 | 0.000110 | 70,028 | 128 | 265 | 1155 Apr. 4, 1962 |
| Au 14 | 0.000090 | 55,979 | 128 | 236 | 1200 Apr. 4, 1962 |
| Au 15 | 0.000105 | 64,781 | 128 | 254 | 1205 Apr. 4, 1962 |
| Au 16 | 0.000110 | 68,203 | 128 | 261 | 1210 Apr. 4, 1962 |

*Cd. covered foil.